https://doi.org/10.5194/hess-2019-359
Preprint. Discussion started: 12 August 2019

Hydrology and Earth System Sciences
Discussions
Open Access
EGU

A novel regional irrigation water productivity model for complex cropping patterns in arid regions coupling soil water and salinity dynamics, irrigation and drainage, and shallow groundwater movement

Jingyuan Xue[1], Zailin Huo[1*], Ian White[2], Isaya Kisekka[3], Zhuping Sheng[4], Shuai Wang[1], Chaozi Wang[1], Guanhua Huang[1], Xu Xu[1]

[1]College of Water Resource and Civil Engineering, China Agricultural University, Beijing 100083, China.

[2]Fenner School of Environment & Society, Australian National University, Fenner Building 141 Canberra ACT 0200.

[3]Univerisity of California Davis, Department of Land, Air and Water Resources and Department of Biological and Agricultural Engineering

[4]Texas A&M University, Agriculture Research and Extension Center, El Paso, USA

[*] Correspondence to: Zailin Huo (huozl@cau.edu.cn)

https://doi.org/10.5194/hess-2019-359
Preprint. Discussion started: 12 August 2019

Hydrology and Earth System Sciences
Discussions

Abstract:

The temporal and spatial distribution of regional irrigation water productivity (RIWP) is crucial for making agricultural related decisions, especially in arid irrigated areas with complex cropping patterns. Thus, we developed a new RIWP model for an irrigated agricultural area with complex cropping patterns. The model couples the irrigation and drainage driven soil water and salinity dynamics and shallow groundwater movement, to quantify the temporal and spatial distributions of the target hydrological and biophysical variables. We divided the study area into 1 km×1km hydrological response units (HRUs). In each HRU, we considered four land-use types: sunflower fields, wheat fields, maize fields and uncultivated lands. And we coupled the regional soil hydrological processes and groundwater flow by taking a weighted average of the water exchange between unsaturated soil and groundwater under different land-use types. The RIWP model was calibrated and validated using eight years of hydrological variables obtained from regional observation sites in a typical arid irrigation area of North China, Hetao Irrigation District. The model reasonably well simulated soil moisture and salinity, groundwater table depths, salinity, and discharge, and regional evapotranspiration. Sensitivity analysis indicates that soil evaporation coefficient and specific yield are the key parameters for RIWP simulation. The results showed that, from 2006 to 2013, RIWP decreased from maize to sunflower to wheat. It was found that the maximum RIWP can be reached when groundwater table depth is in the range of 2 m to 4 m, regardless of irrigation water depths. This implies the importance of groundwater table control on RIWP. Overall, our distributed RIWP model can effectively simulate the temporal and spatial distribution of RIWP and provide critical water allocation suggestions for decision makers.

Keywords: Arid irrigated area, regional water productivity estimation, shallow groundwater, irrigation process, drainage, cropping patterns

1. Introduction

Under the increasing food demand of growing populations worldwide, water resources is limiting food production in many areas (Kijne et al., 2003; Fraiture and Wichelns, 2010). Especially, in arid and semi-arid regions of the world, where irrigated agriculture accounts for about 90% of the total

https://doi.org/10.5194/hess-2019-359
Preprint. Discussion started: 12 August 2019

Hydrology and Earth System Sciences
Discussions
Open Access
EGU

water use (Jiang et al., 2015; Gao et al., 2017), water deficit and related land salinity are the two major limitations to agricultural production (Williams, 1999; Xue et al., 2018). To maximize agricultural production, the improvement of irrigation water productivity (IWP) is vital (Bessembinder et al., 2005; Surendran et al., 2016). IWP is defined as the crop yield per cubic meter of irrigation water supplied (Singh et al., 2004).

Furthermore, by changing hydrological processes, irrigation and drainage affect water and salt dynamics in crop root zone, and, eventually, crop production (Morison et al., 2008; Bouman et al., 2007). Specifically, RIWP analysis requires the quantification of the complex agro-hydrological processes, including soil water and salt dynamics, groundwater movement, crop water use and crop production.

Various methods have been used to evaluate IWP, such as field measurements (Talebnejad et al., 2015; Gowing et al., 2009), remote sensing (Zwart and Bastiaanssen, 2007), and distributed hydrological models (Singh, 2005; Jiang et al., 2015; Steduto et al., 2009). Field experiments have been widely used to evaluate the effect of water management on IWP (Talebnejad et al., 2015; Gowing et al., 2009), but field experiments are expensive and time consuming, making it unsuitable for regional evaluation of IWP. Conveniently revealing temporal and spatial distributions of evapotranspiration (ET) and crop yields, remote sensing is commonly used to quantify regional IWP (Thenkabail and Prasad, 2008). However, remote sensing is look at seeing the past IWP distribution, but cannot readily predict the impacts of water management practices on IWP.

Recently, distributed integrated crop and hydrologic models have been widely used to simulate the complex agro-hydrological processes coupled with salt dynamics and crop production (Aghdam et al., 2013; Noory et al., 2011; van Dam, 2008; Vanuytrecht et al., 2007). Taking advantages of geographic information systems (GIS), distributed integrated crop and hydrologic models provide precise simulations of regional hydrological processes and crop growth, by incorporating the heterogeneity of soil moisture, salinity and texture, groundwater table depth and salinity, and cropping patterns (Amor et al., 2002; Bastiaanssen et al., 2003a; Jiang et al., 2015; Nazarifar et al., 2012; Xue et al., 2017).

There are two types of distributed hydrologic models that are used to integrate with crop models: numerical distributed models, such as SWAT and MODFLOW, and simplified distributed models

https://doi.org/10.5194/hess-2019-359
Preprint. Discussion started: 12 August 2019

based on water balance equations. MODFLOW is commonly used for groundwater dynamics simulation (Kim et al., 2008). But it is limited in well-monitored large irrigation areas, due to the large number of parameters and input data required. SWAT is used to simulate land surface hydrologic and crop growth processes. It relies on the digital elevation model (DEM) to delineate surface water flow pathways. However, many irrigation areas are quite flat, and surface water flow pathways are controlled by irrigation and drainage systems, instead of terrain elevation differences. Furthermore, SWAT alone does not describe the complex interactions between groundwater and soil water, which are fundamental in arid and semi-arid areas with shallow groundwater.

Simplified distributed models often employ mass balance equations to describe the soil water and salt dynamics (Sharma, 1999; Sivapalan et al., 2015), which means less input parameters, and larger spatial grids and temporal steps. However, the large spatial grids can hardly reflect the regional complex cropping pattern heterogeneity, and the large temporal steps cannot capture daily soil water and salt dynamics which is essential for crop growth simulation.

After all, there are still two big challenges for developing a distributed integrated irrigation water productivity models in irrigation areas. First, the networks of irrigation canals and drainage ditches cause spatial heterogeneity in irrigation, drainage, deep percolation, canal seepage and groundwater table depth within the irrigation area. But previous studies have overlooked the important role of the networks of irrigation canals and drainage ditches in RIWP evaluations. Second, the multi-scale matching problem comes out when coupling unsaturated and saturated zone in irrigation areas with complex cropping patterns, as the spatial heterogeneity of cropping patterns is much stronger than that of groundwater table depth. However, most of the existing distributed hydrological models simulated the hydrological processes within the same hydrological response unit (HRU) between unsaturated and saturated zones independently, but overlooked the lateral exchange of groundwater between adjacent HRUs.

Therefore, the main objectives of our study are to (1) develop a RIWP model framework coupling the irrigation and drainage processes, soil water and salt dynamics, crop water and salt response processes, and lateral movement of groundwater and salt; and (2) analyze the distributed RIWP of the study area and find the effects of crop type, irrigation water depth and groundwater table depth on RIWP.

https://doi.org/10.5194/hess-2019-359
Preprint. Discussion started: 12 August 2019

2. Methods

We will present a four-module integrated RIWP model, the coupling between the modules and one case study evaluating the model performance.

2.1 Regional irrigation water productivity model

General descriptions will be given for the four modules and their integration, as well as the division and connections of HRUs, and boundary conditions of the model. Then, detailed descriptions will be given for each of the four modules: irrigation system module, drainage system module, groundwater module, and field scale IWP module.

2.1.1 General descriptions

A four-module integrated RIWP model was developed, to simulate the complex system including water supply from irrigation open canals, field crop water consumption, groundwater drainage into open ditches, and groundwater lateral flow.

(1) Four modules and their integration

The developed RIWP model couples an irrigation system module, a drainage system module, a groundwater module and a field scale IWP evaluation module (Fig. 1). The irrigation system module simulates the water flow along canals and the canal seepage to groundwater (the recharge of the groundwater module), and it provides the amount of water available for field scale irrigation. The drainage system module simulates the drainage to main drainage ditches from groundwater, and this is the discharge of the groundwater module. The groundwater module is used to simulate the groundwater lateral movement, the groundwater boundary for field scale water-salt balance processes, and the groundwater level dynamics for the drainage module. In the field scale IWP module, vertical movement of water and salt in soil profile is simulated, to obtain the soil moisture and salinity of the crop root zone, and to calculate field scale irrigation water productivity. This module provides deep percolation to the groundwater module and obtains capillary rise to soil from the groundwater module. The above mentioned four modules will be described comprehensively in 2.1.2 to 2.1.5.

https://doi.org/10.5194/hess-2019-359
Preprint. Discussion started: 12 August 2019

(2) Hydrological response units

The irrigation area is spatially heterogeneous in terms of soil, land use, meteorology and groundwater. To include the spatial heterogeneities in the simulation of regional water and salt dynamics and its impact on crop growth, the irrigation district was divided into hydrological response units (HRUs) (Kalcic et al., 2015). In each HRU, soil texture and groundwater conditions are assumed to be homogeneous, but different cropping patterns can exist. For example, sunflower fields, wheat fields, maize fields and uncultivated lands. As the irrigation quota is different for different cropping patterns, the model first run field IWP model for each cropping pattern independently in each HRU, to obtain the soil water and salt dynamics, IWP, and groundwater recharge. Then, the groundwater levels and salinity of each HRU can be updated according to the area proportions of different cropping patterns in each HRU. The groundwater flow is determined by pressure head gradient between adjacent HRUs.

(3) Boundary conditions

The upper boundary of the model is the atmospheric boundary layer above the plant canopy, which determines reference ET, and precipitation. The main irrigation canals and drainage ditches directly connect with groundwater and can be considered as the side boundaries in the model. With the canal conveyance water loss deducted from the gross water supplied, the amount of water diverted into the field can be calculated as the actual amount of irrigation. The local irrigation schedules of different crops and the actual time of canal water supply are both considered to determine the actual irrigation time and irrigation amounts. The lower boundary is the confining bed at the bottom of phreatic layer. The phreatic layer is vitally important due to its vertical exchange with the unsaturated soil zone in each HRU and its lateral exchange with adjacent HRUs to bond the whole region together.

2.1.2 Irrigation system module

When irrigation water passes through canals, no matter lined or unlined, seepage loss occurs which recharges groundwater. In a large irrigation area, there are many main, sub-main, lateral, and field canals, which are categorized as the first-, second-, third-, and fourth-order canals, respectively. During the water allocation period, canal seepage loss from different levels of

https://doi.org/10.5194/hess-2019-359
Preprint. Discussion started: 12 August 2019


Hydrology and Earth System Sciences
Discussions

canals can be divided into two parts. One part is the seepage loss from the main and sub-main canals, which are permanently filled with water and recharge directly into groundwater along the route. The other part is the seepage loss from lateral and field canals, which are intermittently filled with water and only recharge the groundwater units within their control area. Each HRU has its corresponding groundwater unit, which is used when calculating lateral exchange of groundwater between adjacent HRUs.

We calculated the decreasing water flow along canal, and water losses in main and sub-main canals as follows (Men 2000):

$$\sigma = \frac{A}{100Q^m} \quad (1)$$

$$\sigma = \frac{dQ}{Qdl} \quad (2)$$

where σ represents the water loss coefficient per unit length per unit flow in canal (m^{-1}). A is the soil permeability coefficient of canal bed ($m^{3m-1}day^{-m}$), m is the soil permeability exponent of canal bed (-), and their values depend on the soil type of the canal bed (please refer to Guo (1997) for the values). Q represents the daily net flow in canal (m^3day^{-1}), and dQ represents the daily flow loss of the water conveyance within dl distance in canal (m^3day^{-1}).

Thus, Eq. (1) is equal to Eq. (2), and they can be transformed into:

$$Q^{m-1}dQ = Adl \quad (3)$$

Integrations of both sides of Eq. (3) gives:

$$\int_{Q_L}^{Q_g} Q^{m-1}\, dQ = \int_0^L A\, dl \quad (4)$$

$$Q_L = ({Q_g}^m - ALm)^{1/m} \quad (5)$$

where Q_g is the daily gross flow in the head of canal (m^3day^{-1}), and Q_L is the daily net flow in canal at L distance away from canal head (m^3day^{-1}). Thus, flow loss in water conveyance process can be calculated as follows:

$$Q_{Ls} = \frac{A}{100}({Q_g}^m - ALm)^{(1-m)/m} \quad (6)$$

$$W_{ls} = Q_{ls}/(n_1 \times A_{su}) \quad (7)$$

where Q_{Ls} is the daily groundwater recharge due to water conveyance loss in main and sub-main canals (m^3day^{-1}), W_{ls} is the groundwater recharge per unit area due to water conveyance loss in main and sub-main canals (m). n represents the total number of HRUs along selected main and

https://doi.org/10.5194/hess-2019-359
Preprint. Discussion started: 12 August 2019

Hydrology and Earth System Sciences
Discussions
Open Access
EGU

sub-main canals (-), and A_{HRU} is the area of each HRU (m^2).

For lateral and field canals, they are intermittently filled with low water flow and are densely distributed in the irrigated area. Thus, it is assumed that seepage from these canals uniformly recharges groundwater units within their control area. The canal seepage is estimated by an empirical formula:

$$W_{as} = I_n * \eta_{mc} * (1 - \eta_{sbmc}) + I_n * \eta_{mc} * \eta_{sbmc} * (1 - \eta_{lc}) + I_n * \eta_{mc} * \eta_{sbmc} * \eta_{lc} * (1 - \eta_{fc}) \quad (8)$$

where W_{as} represents daily groundwater recharge per unit area due to water conveyance loss in lateral and field canals (m), and I_n is daily irrigation water depth per unit area (m). η_{mc}, η_{sbmc}, η_{lc} and η_{fc} are the utilization coefficient of main, sub-main, lateral and field canals, respectively (-).

2.1.3 Drainage system module

In the drainage system module, only the groundwater drainage into ditches is considered. Because the precipitation directly on ditches is negligible in arid and semi-arid area. The drainage processes are simulated based on the spatial distributions of main, sub-main, and lateral ditches, which are grouped into the first-, second-, and third-order ditches, respectively. Drainage is estimated by comparing local groundwater levels and ditch bottom elevation. According to Tang et al. (2007), the groundwater drainage was calculated by:

$$D_g = \begin{cases} \gamma_d \times (h_{db} - h_g) & ; \ h_{db} > h_g \\ 0 & ; \ h_{db} < h_g \end{cases} \quad (9)$$

where D_g is groundwater drainage per unit area (m). γ_d is drainage coefficient (-), which describes the groundwater table decline caused by the elevation difference between groundwater table and the streambed of the drainage ditch. And it depends on the underlying soil conductivity and the average distance between the drainage ditches. h_g represents the groundwater table depth (m), and h_{db} is the streambed depth of drainage ditch (m).

2.1.4 Groundwater module

For a plain irrigation area, usually groundwater levels are relatively flat on a large scale. In our model, it is assumed that groundwater lateral flow exists between one HRU and its four adjacent

https://doi.org/10.5194/hess-2019-359
Preprint. Discussion started: 12 August 2019

Hydrology and Earth System Sciences
Discussions
Open Access
EGU

HRUs (Fig. 2). Using water table gradient, groundwater flow between current HRU and its adjacent HRUs can be calculated by:

$$W_{gr} = (K \times h \times B \frac{L_{ga} - L_g}{D})/\mathrm{B}^2 \quad (10)$$

where W_{gr} is the daily groundwater inflow of the current HRU from adjacent HRUs (m), and K is the permeability coefficient of unconfined aquifers in the current HRU (m). h represents the thickness of unconfined aquifers, which is the difference between water table and upper confined bed and varies with water table changes (m). B is the length of groundwater unit (m) and here the value is 1km. L_{ga} and L_g represents the water table level of adjacent HRUs and the current HRU, respectively (m). D is the distance between the center of the current HRU and the centers of its adjacent HRUs (m). There are three types of groundwater boundaries: river boundaries, drainage ditch boundaries and no flux boundaries.

Based on the field scale simulation, groundwater lateral exchange, canal seepage and groundwater drainage are added in the daily water and salt balance calculations of each groundwater unit at regional scale:

$$hg_i = hg_{i-1} - (1/S_y)(Pwg_{i-1} - Gwg_{i-1} - ext_{i-1} + W_{grupi-1} + W_{grdowni-1} + W_{grlefti-1} + W_{grrighti-1} + W_{lsi-1} + W_{asi-1} - D_{gi-1}) \quad (11)$$

$$SCa_i = Za \times Sa_{i-1} + \mathrm{W}_{grupi-1} \times Sa_{upi-1} + \mathrm{W}_{grdowni-1} \times Sa_{downi-1} + \mathrm{W}_{grlefti-1} \times Sa_{lefti-1} + \mathrm{W}_{grrighti-1} \times Sa_{righti-1} + (\mathrm{W}_{lsi-1} + \mathrm{W}_{asi-1}) \times Is_{\mathrm{i}-1} - \mathrm{D}_{gi-1} \times Sa_{\mathrm{i}-1} + Psg_{i-1} - Gsg_{i-1} \quad (12)$$

where W_{grup}, W_{grdown}, W_{grleft} and $W_{grright}$ are the daily groundwater lateral runoff per unit area into the current groundwater unit from up and down or left and right adjacent groundwater unit, respectively (m). SCa is the soluble salt content in the saturated zone below the transmission soil profile (mg m^{-2}). Z_a is the thickness of the saturated zone which is the difference between the groundwater table depth and the depth that groundwater table fluctuations largely cannot reach (m). Z_a only affect the soluble salt concentration in the groundwater salt balance, while it has no effect on the water balance and groundwater fluctuation simulation. Sa, Sa_{up}, Sa_{down}, Sa_{left} and Sa_{right} is the salt concentration of the current groundwater unit and its up and down or left and right adjacent groundwater units, respectively (mg m^{-3}). Is is the salt concentration of the irrigation water (mg m^{-3}). S_y represents the specific yield (-), which is the ratio of the volume of water that can be drained

https://doi.org/10.5194/hess-2019-359
Preprint. Discussion started: 12 August 2019

by gravity to the total volume of the saturated soil/aquifer. *ext* is the daily groundwater extraction per unit area (m). P_{wg} is the daily percolation water depth to groundwater from the potential root zone (m), and G_{wg} is the daily water depth supplied to the potential root zone from shallow groundwater due to the rising capillary action (m). P_{sg} and G_{sg} are the quantity of soluble salt in P_{wg} and G_{wg}, respectively (mg m^{-2}). The detailed calculations of the water and salt exchange components between unsaturated soil and groundwater, such as P_{wg} and G_{wg}, were described in our previously developed water productivity model at field scale (Xue et al., 2018).

2.1.5 Field scale irrigation water productivity module

Cropping patterns are complex for each HRU and sometimes HRU include uncultivated land, forest land and other non-agricultural land. In our model, with high resolution land use map, different cropping patterns can be separated to simulate soil water and salt processes, and the responses of ET and crop yields to water and salt content of root zone. Here, we employed our previously developed field IWP model to simulate field water, salt, ET and crop yield under shallow groundwater condition (Xue et al., 2018). The soil profile is vertically divided into four soil zones: the current root zone, the potential root zone, the transmission zone, and the saturated zone. In each HRU, the soil water and salt balance processes, and water productivity are independently simulated for each cropping pattern under its corresponding groundwater unit condition. For uncultivated lands, only water and salt balance are simulated, and its IWP is 0. Then, the water and salt exchange between unsaturated soil and groundwater of different cropping patterns are weighted averaged by area proportion. Finally, the weighted averages are used to updated daily groundwater table and salinity (Fig. 3).

2.2 Modules coupling and calculating flowchart

The simulation was by daily temporal step and by HRU spatial step. The irrigation system module simulates the canal seepage to groundwater and the field irrigation water amount. And the canal seepage to groundwater is the recharge of the groundwater module, while the field irrigation water amount is the input of the field IWP module. The drainage system module simulates the groundwater drainage to drainage ditches, which is the discharge of the groundwater module. The

https://doi.org/10.5194/hess-2019-359
Preprint. Discussion started: 12 August 2019


Hydrology and Earth System Sciences
Discussions

groundwater module is used to simulate the groundwater table depth, which is the input of the field IWP module and also the input of the drainage module. In the field scale IWP module, the deep percolation to groundwater under different cropping patterns are simulated independently and their weighted average is the recharge of the groundwater module. The salt exchange is simulated together with water exchange. The groundwater module is used to simulate the groundwater lateral movement between the current HRU and its adjacent HRUs to update the groundwater level at next time step. By coupling the irrigation system module, drainage system module and groundwater module with the field IWP model, this RIWP model simulates the temporal and spatial distribution of IWP in the whole irrigation area from the beginning to the end of the growing season.

The model was implemented in a combination of ArcGIS, MATLAB, and Microsoft Excel (Fig. 4). The HRUs was created in ArcGIS as fishnet, with each grid numbered. In MATLAB, the HRUs were represented by a matrix and the daily time step was represented by a vector. At each time step, all the HRUs were traversed by a nested loop. Then the updated information for the current time step was used to calculate the next time step. Microsoft Excel stored ArcGIS vector layer and its attribute data for MATLAB modeling, and also stored MATLAB output results for ArcGIS analysis and visualization.

Considering spatial heterogeneity, meteorological data need to be collected from all the weather stations within or close to the study area. Soil physical properties, moisture and salinity distribution in unsaturated soil, and groundwater table depth and salinity need to be collected from many observation sites uniformly or randomly covering the study area. Then, each data set can be interpolated in ArcGIS by inverse distance weight to obtain a spatial distribution vector layer. For each layer, the average value in each HRU are calculated by ArcGIS using geometric division statistics. The vector layer of irrigation control zones and the vector layer of drainage control zones is respectively overlaid with the HRU division layer in ArcGIS, to obtain the HRU numbers controlled by each irrigation control zone and each drainage control zone. The HRU numbers controlled by the same zone are stored in the same matrix for batch simulation in MATLAB. In MATLAB, soil water and salt balances and field scale IWP for main crops are simulated simultaneously for each HRU; whereas, groundwater lateral exchange are simulated between adjacent HRUs. At the end of the model simulation, soil moisture and salinity, groundwater table

https://doi.org/10.5194/hess-2019-359
Preprint. Discussion started: 12 August 2019

depth and salinity, ET, crop yield and IWP for different land use types in each HRU can be obtained. Then, the area proportion weighted average in each HRU can be imported into ArcGIS to visualize the spatial distribution.

2.2 Model evaluation

We will provide a case study using the above developed new RIWP model, to test its applicability, and to provide sensitivity analysis of the parameters.

2.3.1 Description of study area and data

As a typical sub-district of the Hetao Irrigation District, the Jiefangzha Irrigation District (JFID) is a typical arid irrigation area with shallow groundwater, resulted from its arid continental climate, flood irrigation year after year, and desperate drainage systems (Fig. 5). Located in the Hetao Plain, the JFID is very flat with an average slope of 0.02% from southeast to northwest (Xu et al., 2011). The mean annual precipitation is only 155 mm, of which 70% occurs between July to September; while the mean annual potential evaporation is 1938 mm. The mean annual temperature is 7°C, with the lowest and highest monthly average being −10.1°C and 23.8°C in January and July, respectively. The JFID covers an area of 1.12 Mha, of which 66% is irrigated farmland area. Wheat, maize and sunflower as the main crops in this region, taking up more than 90% of the irrigated farmland area. The 12×10^8 m^3 annual irrigation water is diverted from the Yellow River. Due to the poor maintenance of drainage ditches, it is quite common in this area to have poor drainage situations. Therefore, the annual average groundwater table depth ranges from 1.5 to 3.0 m during the crop growing season. Soils in the JFID are spatially heterogeneous and primarily composed of silt loam in the northern region and sandy loam in the southern region. Shallow groundwater table and strong evaporation makes soil salinization a very serious problem in this area, which is becoming the main constraint of crop production.

An irrigation and drainage network include four main irrigation canals, sixteen sub-main irrigation canals, five main drainage ditches, and twelve sub-main drainage ditches are controlling the water movement in the JFID (Fig. 5). The streambed depths of the regional main, sub-main and lateral ditches were collected by a regional survey in 2006. Daily water flow data in the main and sub-main

https://doi.org/10.5194/hess-2019-359
Preprint. Discussion started: 12 August 2019


Hydrology and Earth System Sciences
Discussions

irrigation canals and monthly data of the five main drainage ditches were obtained from the local Irrigation Administration Bureau. A total of 55 groundwater observation wells are installed in the JFID (Fig. 5). Groundwater level was measured on the 1st, 6th, 11th, 16th, 21th and 26th of each month, and groundwater salinity was measured 3 times each month. Near the groundwater observation wells, soil moisture was measured four times, and soil electrical conductivity was measured once before wheat sowing and once before autumn irrigation. Due to the spatially homogeneous climate in JFID, daily meteorological data (air temperature, humidity, wind speed and precipitation) was obtained from Hangjinghouqi weather station for the calculation of regional reference ET.

HJ-1A, HJ-1B and Landsat NDVI images with 30 m resolution during the period of 2006-2013 were downloaded from the official website of China Centre for Resources Satellite Data and Application (2013) and USGS (2013), to determine the annual cropping pattern distributions. Due to the lack of measured ET, the ET estimated by SEBAL model using MODIS images from NASA (2013) was used as a reference to compare with simulated ET values (Bastiaanssen et al., 2003b).

2.3.2 Model application

The JFID was divided into 2485 1km×1km HRUs (Fig. S1a in the supplementary material). In terms of boundary conditions, the upper Quaternary 4 aquifer layer was regarded as the phreatic layer in the model. It was modeled as an aquitard with loamy soil. From north to south, the thickness of aquifer in JFID varies from 2 to 20m with an average of 7.4m (Bai et al., 2008). Thus, the initial value of the average thickness of unconfined aquifer is set as 7.4m. The water level contour maps of JFID during 1997-2002 by Bai (200) were used to determine the direction of water flow near the groundwater boundary. Based on the topography conditions, land-use types, locations of main canals and ditches, and directions of water flow, the regional phreatic layer was divided into 5 zones with river, drainage and impervious boundary conditions (Fig. S1b).

The JFID was divided into four irrigation control sections and five drainage control sections, each section was controlled by one main irrigation canal or one main drainage ditch. These sections were further divided into 48 irrigation control sub-areas and 17 drainage control sub-areas, each sub-area was controlled by one sub-main irrigation canal or one sub-main drainage ditch (Fig. S2). The sunflower fields, wheat fields, maize fields and uncultivated lands are the four cropping patterns,

https://doi.org/10.5194/hess-2019-359
Preprint. Discussion started: 12 August 2019

i.e., land-use types, in the RIWP model. The irrigation time and irrigation water amount of each HRU were determined by both the local irrigation schedule of the three main crops, and the actual water amount flowing into the fields.

The simulation period was from April 1st to September 20th, coving the growing season of all the three main crops. The initial crop parameters were set as the default values suggested for sunflower, wheat, and maize by Allen et al. (1998). The empirical values of regional canal utilization and ditch drainage coefficient were obtained from Jiefangzha administration.

To comprehensively evaluate the accuracy and reliability of the model, the data in years 2010-2013 and in years 2006-2009 was respectively used as calibration and validation dataset. The soil moisture content of root zone (θ), electrical conductivity of soil water (EC), groundwater table depth (h_g) and groundwater salinity, were calibrated with measured data from the 22 soil water and salt observation sites and 55 groundwater observation sites (Fig. 5). The RIWP simulated regional ET was calibrated by the ET data obtained from remote sensing images once per 8 days. The regional drainage processes was calibrated by the monthly groundwater drainage data from main ditches. Overall, the soil hydraulic parameters, the crop water productivity related coefficient, and the canal conveyance and ditch drainage parameters were all calibrated with observed data in years 2010-2013, and then validated with observed data in years 2006-2009.

To quantify the model performance, the root mean square error (RMSE), the Nash and Sutcliffe model efficiency (NSE) and the coefficient of determination (R^2) were used as the indicators. RMSE was used to measure the deviation of simulated values from the measured ones, NSE was commonly used to verify the credibility of the hydrological model, and R^2 represented the degree of linear correlation. The indicators were calculated as follows:

$$RMSE = \left[\frac{\sum_{i=1}^{n}(Output_s - Output_o)^2}{n}\right]^{0.5} \quad (13)$$

$$NSE = 1 - \frac{\sum_{i=1}^{n}(Output_s - Output_o)^2}{\sum_{i=1}^{n}(Output_o - Output_m)^2} \quad (14)$$

$$R^2 = 1 - \frac{\sum_{i=1}^{n}(Output_o - \overline{Output_o})(Output_s - \overline{Output_s})}{\sqrt{\sum_{i=1}^{n}(Output_o - \overline{Output_o})^2}\sqrt{\sum_{i=1}^{n}(Output_s - \overline{Output_s})^2}} \quad (15)$$

where n is the number of simulations; $Output_s$ and $Output_o$ are simulated and observed values of model outputs, respectively; $\overline{Output_s}$ and $\overline{Output_o}$ are the average values of simulated and

https://doi.org/10.5194/hess-2019-359
Preprint. Discussion started: 12 August 2019

observed model outputs, respectively. A model performs well when *NSE* and R^2 are close to 1, and *RMSE* is close to 0, indicate good model performance. For *NSE*, particularly, a zero value means that the prediction is not better than taking an average, and a negative value means that the prediction is worse than taking an average.

2.3.4 Global sensitivity analysis

To find the key parameters significantly impacting the model output, a global sensitivity analysis was conducted. The analysis related the changes in three output variables—RIWP, groundwater table depth and groundwater salinity—to eight parameters in the RIWP model. The Latin Hypercube Sampling (LHS) (please see Mckay, 1979; Muleta et al., 2005; Wang et al., 2008 for detailed descriptions of the sampling method), a typical sampling method for sensitivity and uncertainty analysis, was used to sample the parameter space. According to Dai (2011), to ensure that the test points were evenly distributed in space and to guarantee the accuracy of the test, the test number was set as 20, more than double of the parameter number which was 8. Additionally, considering the spatial heterogeneity of the three output variables, 22 evenly distributed groundwater observation sites in JFID were selected for the global sensitivity analysis. Based on the LHS method, 20 groups of parameter combinations were obtained and the simulation was run for 20 times. Finally, the sensitivity of the three output variables to the eight parameters were determined in SPSS Statistics. The absolute values of the obtained Standardized Regression Coefficients (SRCs) quantified the significance of each parameter to each output variable (Table 1) (Cheng et al., 2018; Cannavó, 2012). And the plus or minus sign of the SRCs indicated the positive or negative correlations between the corresponding parameter and output variable pairs.

3. Results and Discussion

3.1 Model performance

Table 2 tabulated the calibrated parameters describing crop growth and water usage, and Table 3 tabulated the variation range and calibrated values of the parameters describing soil hydraulic characteristics and irrigation and drainage system. The agreement between the observed and simulated soil moisture content in crop root zone both in calibration (Fig. 6a, *RMSE*=2.867 cm cm^{-}

https://doi.org/10.5194/hess-2019-359
Preprint. Discussion started: 12 August 2019

415 ^{3}, *NSE*=0.330, R^2=0.502) and validation (Fig. 6b, *RMSE*=2.989 cm cm^{-3}, *NSE*=0.232, R^2=0.548)
416 indicates the good performance of the RIWP model. The good performance of the RIWP model was
417 also indicated by the simulation of the soil salt content both in calibration (Fig. 6c, *RMSE*=2.867 cm
418 cm^{-3}, *NSE*=0.612, R^2=0.657) and validation (Fig. 6d, *RMSE*=1.205 dS m^{-1}, *NSE*=0.525, R^2=0.590).
419 The simulated and observed groundwater table depth (Fig. 6e, *RMSE*=0.786m, *NSE*=0.424 and
420 R^2=0.509 in calibration; Fig. 6f, *RMSE*=0.667m, *NSE*=0.637 and R^2=0.504 in validation) and
421 groundwater salinity (Fig. 6g, *RMSE*<10%, *NSE*=0.813 and R^2=0.815 in calibration; Fig. 6h,
422 *RMSE*<10%, *NSE*=0.604 and R^2=0.730 in validation) at 55 observation sites are in good agreement
423 as well.
424 The overestimated drainage (Fig. 6i-j) was due to the different operating conditions of the drainage
425 ditches of the same order. Remember that we classified the main, sub-main and lateral drainage
426 ditches into the first-, second and third-order ditches, respectively. In the model, for each year, all
427 the ditches of the same order share the same the drainage coefficient, assuming a well operated
428 condition. However, the actual operating conditions of the ditches of the same order cannot be the
429 same, resulting in the simulation discrepancy.
430 The ET simulated by the RIWP model (ET_{IWP}) and the ET estimated by the SEBAL model using
431 MODIS images (ET_{RS}) agrees well both in calibration (RMSE=1.918mm, *NSE*=0.274 and R^2 =
432 0.561) and in validation (RMSE=2.132mm, *NSE* =0.189 and R^2 =0.498) (Fig. 6l). Furthermore, the
433 comparison of the spatial distribution of cumulative ET_{IWP} and ET_{RS} during crop growth season
434 showed that ET_{IWP} was lower than ET_{RS} in uncultivated area, while they agreed well in farmland
435 (Fig. S3). The uncultivated area, merely bare soil, accounted for about 34% of the JFID, and the
436 ET_{IWP} of uncultivated area was merely soil evaporation. This , resulted in the underestimation of
437 actual ET in uncultivated area compared to the ET acquired by remote sensing images, which was
438 consistent with previous studies (Singh, 2005; Tian et al., 2015).
439 To test the model performances under different cropping patterns, one representative site was
440 selected for each cropping pattern to compare the observed and simulated time series of groundwater
441 table depth (Fig. 7). The model can adequately capture the groundwater dynamics at the four
442 representative sites. Occasionally, the simulated groundwater table depth declines fast, while the
443 observed value rises. This is most likely due to the fact that we ignored the time lag between

https://doi.org/10.5194/hess-2019-359
Preprint. Discussion started: 12 August 2019


Hydrology and Earth System Sciences
Discussions

444 groundwater recharge from soil and deep percolation.

445 **3.2 Global sensitivity analysis**

446 Recall that the global sensitivity analysis was to determine the sensitivity of the three output
447 variables to eight parameters. The three output variables were RIWP, groundwater table depth, and
448 groundwater salinity; while, the eight parameters were those parameters describing soil hydraulic
449 characteristics and irrigation and drainage system, tabulated in Table 3. Specific yield (S_y), followed
450 by soil evaporation coefficient (K_e), are the two key parameters influencing the RIWP (Fig. 8a). The
451 specific yield indicated the readily available groundwater for crop consumption. Thus, its significant
452 positive influence on RIWP was explained. The soil evaporation coefficient indicated the proportion
453 of water that transferred into the atmosphere but was not used by crops. Therefore, its significant
454 negative impact on RIWP was expected. And for both groundwater table depth (Fig. 8b) and
455 groundwater salinity (Fig. 8c), specific yield was the only key parameter. Canal seepage was
456 expected to cause the variation of groundwater table depth around the canal at the local scale.
457 However, the results indicated that the variation of groundwater table depth would be more
458 susceptible to the local groundwater properties, i.e., specific field, than to canal seepage at the
459 regional scale. We speculate that the lateral groundwater movement might compensate the variation
460 of groundwater table depth caused by the canal seepage. Salt moves with water. Thus, the variation
461 of groundwater salinity was also dominated by the specific yield .

462 **3.3 Regional irrigation water productivity**

463 **3.3.1 Spatial distribution of irrigation water productivity**

464 Validated by the measured soil moisture and salinity, groundwater table depth and salinity, drainage
465 water depth and ET, especially, the year 2006-2013 time series of groundwater table depth under
466 the four cropping patterns, the developed RIWP model can be used to estimate the spatial
467 distribution of IWP for the three main crops over the period of 2006-2013 (Fig. 9). The RIWP of the
468 three main crops showed a trend of decline during the period of 2006-2010 (Fig. 9a-e).This was
469 mainly attributed to the increasing irrigation quota, as the excess water lowered the IWP. Whereas,

https://doi.org/10.5194/hess-2019-359
Preprint. Discussion started: 12 August 2019


Hydrology and Earth System Sciences
Discussions

during the period of 2011-2013 (Fig. 9f-h), the RIWP of the three main crops showed an increasing trend. This was because that the irrigation quota was reduced over this period, and the contribution of groundwater compensated the crop yield losses.

Under a given irrigation water distribution, the spatial distribution of ET was the key factor controlling the RIWP distribution. And the spatial distribution of ET was fundamentally determined by the solar energy, and the water and salt dynamics of soil. Recall that the climate and, therefore, the solar energy, was homogeneous in JFID. Then, the spatial heterogeneity of RIWP must be attributed to the water and salt heterogeneity caused by the spatial heterogeneity of the cropping pattern, groundwater table depth, and irrigation and drainage networks. Particularly, when the farmlands had limited supply of irrigation water, the groundwater table depth and salinity played an important role on IWP.

The comparison between the RIWP of different crops (comparing the three columns in Fig. 9) showed that maize had the highest IWP, wheat had the lowest IWP, and the IWP of sunflower was in the middle. Therefore, modestly increasing the planting area of maize will improve the crop production per unit irrigation water amount. In addition, the RIWP of sunflower is a little higher than that of wheat, and the benefit and the salt tolerance of sunflower are both much higher than those of wheat. Thus, planting sunflowers should be promoted in the JFID.

3.2.2 The impact of irrigation water depth and groundwater table depth on irrigation water productivity

In arid shallow groundwater area, irrigation water productivity (IWP) is affected by irrigation water depth (IWD) and groundwater table depth (h_g). In all the four simulated h_g ranges, IWP decreased when IWD increased (Fig. 10a), which was consistent with Huang et al. (2005). Moreover, the magnitude of IWP decrease per unit increase of IWD was different under different h_g ranges. The magnitude of IWP decrease under shallower h_g was smaller than that under deeper h_g. This effect of increasing h_g on the relationship between IWP and IWD was consistent with Gao et al. (2017). The above results indicate that when irrigation water is insufficient, groundwater can compensate the crop water demand. However, when irrigation water is excessive, a large proportion will eventually drain through the drainage ditches, and the IWP drops. Additionally, among the four h_g ranges, the

https://doi.org/10.5194/hess-2019-359
Preprint. Discussion started: 12 August 2019


Hydrology and Earth System Sciences
Discussions

498 highest IWP was obtained in the range of 2-3m (Fig. 10b), which was consistent with Xue et al.
499 (2018). This indicates that a h_g deeper than that provides insufficient water for crop growth; whereas,
500 a h_g shallower than that will increase root zone soil salinity and salt stress of crops. The negative
501 effect of shallow groundwater salinity can also be found in Fig. 10a when h_g is less than 2m, and it
502 indicates that irrigation applied decreasing from 300<IWD<400mm to 200<IWD<300mm lead to
503 not increase but slightly decrease of IWP, which is caused by more reduction of ET. Shallow buried
504 groundwater contribution will make up for ET reduction when smaller irrigation water applied, thus
505 there exists another reason accelerate the reduction of ET, which is less irrigation water will weaken
506 the role of irrigation on salt leaching and result in more severe salinization in crop root zone. Thus,
507 reasonably determining the irrigation quota and constantly maintaining the drainage system to keep
508 the groundwater table depth in the optimal range is of great importance to reach higher crop IWP at
509 the regional scale.

510 4. Conclusions

511 In view of the particularity of irrigated areas, taking fully consideration of the supply,
512 consumption and drainage processes of irrigation water and groundwater, a distributed RIWP
513 model was developed to couple the irrigation water flow processes along main canals and drainage
514 processes, water and salt transport processes in soil profile, groundwater water and salt lateral
515 transport, and agricultural water productivity module. Especially, a new method was designed and
516 incorporated to couple regional soil hydrology process and groundwater flow, with the spatial
517 difference of cropping pattern. Taking advantages of remote sensing and GIS tools, the
518 quantitative distributed RIWP model needs fewer soil and groundwater hydraulic parameters and
519 crop growing parameters and only readily available data of several observation sites at the
520 regional scale, and regional water and salt process can be simulated on a daily time step. Despite
521 the simplifications involved, the proposed methods of irrigation canal and drainage ditches
522 digitization and groundwater-runoff lateral exchange simulation between grids make the spatial
523 IWP simulation in a real distributed way, instead of using a field scale model applied in a
524 distributed mode to simulate all simulation units independently. The calibration and validation
525 results indicates a good performance of RIWP model applied in this typic study area, and spatial

https://doi.org/10.5194/hess-2019-359
Preprint. Discussion started: 12 August 2019

526 distribution of IWP for different crops can be produced.

527 Data availability

528 The simulation results of the water budget during the simulation period of the JFID in this study
529 are available from the authors upon request (jiyxue@ucdavis.edu).

530 Author contributions

531 JYX and ZLH developed the idea to develop the conceptual RIWP model for irrigated area in arid
532 region with shallow groundwater and complex cropping patterns. JYX wrote the programming
533 code of the RIWP model in Matlab. JYX collected and processed the multiple datasets with the
534 help of SW, GHH and XX and prepared the paper. The results were extensively commented on
535 and discussed by ZLH, IW, IK, ZPS, and CZW.

536 Competing interests

537 The authors declare that they have no conflict of interest.

538 Acknowledgements

539 This study was supported by the National Key Research and Development Program of China
540 (2017YFC0403301), the National Natural Science Foundation of China (51679236, 51639009)
541 and the International Postdoctoral Exchange Fellowship Program from the Office of China
542 Postdoctoral Council (20180044). Special thanks also go to the adminstration of Hetao Irrigation
543 District and Shahaoqu experimental station for providing information and data.

544 Reference

545 Aghdam, E. N., Babazadeh, H., Vazifedoust, M., Kaveh, F., 2013. Regional modeling of wheat
546 yield production using the distributed agro-hydrological swap. Advances in Environmental
547 Biology, 7(7).
548 Amor, V.M., Ashim, D.G., Rainer, L., 2002. Application of GIS and crop growth models in
549 estimating water productivity. Agricultural Water Management, 54, 205–225.
550 Bai, Z. 2008. Numerical simulation and analysis of the groundwater and salt dynamics in
551 Jiefangzha irrigation scheme of Hetao irrigation district. (Master Dissertation). China
552 Agricultural University. (In Chinese)
553 Bai, Z., Xu, X., 2008. Numerical simulation of the groundwater and salt dynamics in Jiefangzha

https://doi.org/10.5194/hess-2019-359
Preprint. Discussion started: 12 August 2019

554 irrigation scheme of Hetao irrigation district. Water Saving Irrigation (2), 29-31. (In Chinese)
555 Bastiaanssen, W., Ahmad, M. D., Tahir, Z., Kijne, J. W., Barker, R., Molden, D., 2003a.
556 Upscaling water productivity in irrigated agriculture using remote-sensing and gis
557 technologies. Iwmi Books Reports, 289-300.
558 Bastiaanssen, W. G. M., Zwart, S. J., Pelgrum, H., Dam, J. C. V., 2003b. Remote sensing analysis.
559 In Dam, J.C. van, R.S. Malik (Eds.), 2003. Water productivity of irrigated crops in Sirsa district,
560 India. Integration of remote sensing, crop and soil models and geographical information
561 systems. WATPRO final report, including CD-ROM. ISBN 90-6464-864-6: 85-100.
562 Bessembinder, J. J. E., Leffelaar, P. A., Dhindwal, A. S., Ponsioen, T. C., 2005. Which crop and
563 which drop, and the scope for improvement of water productivity. Agricultural Water
564 Management, 73(2), 113-130.
565 Cannavó, F., 2012. Sensitivity analysis for volcanic source modeling quality assessment and
566 model selection. Computers and Geosciences, 44(13), 52-59.
567 CERSDA, 2013. http://www.cresda.com/EN/, last access: 15 November 2017.
568 Dai, Y. B., 2011. Uncertainty analysis of vehicle accident reconstruction results based on Latin
569 Hypercube Sampling. (Doctoral dissertation), Changsha University of Science and
570 Technology. (In Chinese)
571 Fraiture, C. D., Wichelns, D., 2010. Satisfying future water demands for agriculture. Agricultural
572 Water Management, 97(4), 0-511.
573 Gao, X., Huo, Z., Qu, Z., Xu, X., Huang, G., Steenhuis, T. S., 2017. Modeling contribution of
574 shallow groundwater to evapotranspiration and yield of maize in an arid area. Scientific
575 Reports, 7, 43122.
576 Gowing, J. W., Rose, D. A., Ghamarnia, H., 2009. The effect of salinity on water productivity of
577 wheat under deficit irrigation above shallow groundwater. Agricultural Water Management,
578 96(3), 517-524.
579 Guo, Y.,f 1997. Irrigation and Drainage Engineering. China Water Power Press.
580 Huang, Y., Chen, L., Fu, B., Huang, Z., Gong, J., 2005. The wheat yields and water-use efficiency
581 in the loess plateau: straw mulch and irrigation effects. Agricultural Water Management, 72(3),
582 209-222.

https://doi.org/10.5194/hess-2019-359
Preprint. Discussion started: 12 August 2019

583 Kalcic, M. M., Chaubey, I., Frankenberger, J., 2015. Defining soil and water assessment tool (SWAT)
584 hydrologic response units (HRUs) by field boundaries. International Journal of Agricultural &
585 Biological Engineering, 8(3), 69-80.
586 Kijne, J. W., Barker, R., Molden, D. J., 2003. Water productivity in agriculture: limits and
587 opportunities for improvement. Wallingford, UK: CABI, IWMI.
588 Kim, N. W., Chung, I. M., Won, Y. S., Arnold and Jeffrey, G., 2008. Development and application
589 of the integrated SWAT-MODFLOW model. Journal of Hydrology, 356(1-2), 1-16.
590 Mckay, M. D., Beckman, R. J., Conover, W. J., 1979. A comparison of three methods for selecting
591 values of input variables in the analysis of output from a computer code in wsc '05:
592 proceedings of the 37th conference on winter simulation. Technometrics, 21(2), 239-245.
593 Muleta, M. K., Nicklow, J. W., 2005. Sensitivity and uncertainty analysis coupled with automatic
594 calibration for a distributed watershed model. Journal of Hydrology, 306(1), 127-145.
595 NASA, 2013. https://modis.gsfc.nasa.gov/, last access: 18 November 2017.
596 Nazarifar, M., Kanani, M., Momeni, R., 2012. Analysis of spatial and temporal variations in crop
597 water productivity of the rainfed wheat for a regional scale analysis. Agriculture, 58(2), 65-
598 73.
599 Noory, H., S.E.A.T.M. van der Zee, Liaghat, A. M., Parsinejad, M., Dam, J. C. V., 2011.
600 Distributed agro-hydrological modeling with swap to improve water and salt management of
601 the voshmgir irrigation and drainage network in northern iran. Agricultural Water
602 Management, 98(6), 1062-1070.
603 Sharma, B. R., 1999. Regional salt- and water-balance modelling for sustainable irrigated
604 agriculture. Agricultural Water Management, 40(1), 0-134.
605 Singh, O. P., Sharma, A., Singh, R., Shah, T., 2004. Virtual water trade in dairy economy
606 irrigation water productivity in Gujarat. Economic and political weekly, 39(31), 3492-3497.
607 Singh, R., 2005. Water productivity analysis from field to regional scale. (Doctoral Dissertation).
608 Wageningen University.
609 Sivapalan, M., Viney, N. R., Jeevaraj, C. G., 2015. Water and salt balance modelling to predict the
610 effects of land - use changes in forested catchments. 3. The large catchment
611 model. Hydrological Processes, 10(3), 429-446.

https://doi.org/10.5194/hess-2019-359
Preprint. Discussion started: 12 August 2019

612 Steduto, P., Hsiao, T. C., Raes, D., Fereres, E., 2009. Aquacrop--the FAO crop model to simulate
613 yield response to water: i. concepts and underlying principles. Agronomy Journal, 101(3),
614 448-459.
615 Talebnejad, R., Sepaskhah, A. R., 2015. Effect of deficit irrigation and different saline
616 groundwater depths on yield and water productivity of quinoa. Agricultural Water
617 Management, 159, 225-238.
618 Tang, Q., Hu, H., Oki, T., Tian, F., 2007. Water balance within intensively cultivated alluvial
619 plain in an arid environment. Water Resources Management, 21(10), 1703-1715.
620 Thenkabail and Prasad, S., 2008. Water productivity mapping methods using remote
621 sensing. Journal of Applied Remote Sensing, 2(1), 023544.
622 Tian, Y., Zheng, Y., Zheng, C., Xiao, H., Fan, W., Zou, S., et al., 2015. Exploring scale-dependent
623 ecohydrological responses in a large endorheic river basin through integrated surface water-
624 groundwater modeling. Water Resources Research, 51(6), 4065-4085.
625 USGS, 2013. *https://earthexplorer.usgs.gov/*, last access: 18 March 2018.
626 Vanuytrecht, E., Raes, D., Steduto, P., Hsiao, T. C., Fereres, E., Heng, L. K., 2014. Aquacrop:
627 fao's crop water productivity and yield response model. Environmental Modelling &
628 Software, 62, 351-360.
629 Van Dam, J. C., Groenendijk, P., Hendriks, R. F. A., Kroes, J. G., 2008. Advances of modeling
630 water flow in variably saturated soils with SWAP. Vadose Zone J,7(2), 640-653.
631 Wang, H. C., Du, P. F., Zhao, D. Q., Wang, H. Z., Li, Z. Y., 2008. Global sensitivity analysis for
632 urban rainfall-runoff model. China Environmental Science, 28(8), 725-729.
633 Xu, X. 2011. Simulation of hydrological process and its responses to agricultural water-saving
634 practices in Hetao irrigation districts (Doctoral Dissertation). China Agricultural University.
635 (In Chinese)
636 Xue, J., Guan, H., Huo, Z., Wang, F., Huang, G., Boll, J., 2017. Water saving practices enhance
637 regional efficiency of water consumption and water productivity in an arid agricultural area
638 with shallow groundwater. Agricultural Water Management, 194, 78-89.
639 Xue, J., Huo, Z., Wang, F., Kang, S., Huang, G., 2018. Untangling the effects of shallow
640 groundwater and deficit irrigation on irrigation water productivity in arid region: new

https://doi.org/10.5194/hess-2019-359
Preprint. Discussion started: 12 August 2019

conceptual model. Science of the Total Environment, 619-620, 1170-1182.

Zhao, C., Shen, B., Huang, L., Lei, Z., Hu, H.,Yang, S., 2009. A dissipative hydrological model for the hotan oasis (DHMHO). Water Resources Management, 23(6), 1183.

Zwart, S. J., Bastiaanssen, W. G. M., 2007. Sebal for detecting spatial variation of water productivity and scope for improvement in eight irrigated wheat systems. Agricultural Water Management, 89(3), 287-296.

https://doi.org/10.5194/hess-2019-359
Preprint. Discussion started: 12 August 2019

Hydrology and Earth System Sciences
Discussions

Table Captions

Table 1. The significance level of the input parameter to the model output variables

Table 2. Calibrated crop parameters of wheat, sunflower and maize for regional irrigation water productivity model

Table 3. The variation range and calibrated values of the parameters describing soil hydraulic characteristics and irrigation and drainage system.

https://doi.org/10.5194/hess-2019-359
Preprint. Discussion started: 12 August 2019

Hydrology and Earth System Sciences
Discussions
Open Access
EGU

699 Table 1. The significance level of the input parameter to the model output variables

SRC value	Significance level
$0.8 \leq \lvert SRC \rvert \leq 1$	Very important
$0.5 \leqslant \lvert SRC \rvert \leqslant 0.8$	Important
$0.3 \leqslant \lvert SRC \rvert \leqslant 0.5$	Unimportant
$0 \leqslant \lvert SRC \rvert \leqslant 0.3$	Irrelevant

700

701 Table 2. Calibrated crop parameters of wheat, sunflower and maize for regional irrigation water
702 productivity model

Parameters	Calibrated value		
	Wheat	Sunflower	Maize
Rate of yield decrease per unit of excess salts, b (%/(ds/m))	7.1	12	12
Average fraction of TAW that can be depleted from the root zone before moisture stress, p (-)	0.55	0.45	0.55
Crop coefficient at crop initial stage, k_{c1} (-)	0.3	0.3	0.3
Crop coefficient at crop development stage, k_{c2} (-)	0.73	0.8	0.75
Crop coefficient at mid-season stage, k_{c3} (-)	1.15	1	1.2
Crop coefficient at last season stage, k_{c4} (-)	0.4	0.7	0.6
Yield response factor, K_y (-)	1.15	0.95	1.25
Electrical conductivity of the saturation extract at the threshold of EC_e when crop yield firstly reduces below Y_m at last season stage, EC_{et} (dS/m)	5	1.7	2

703

704 Table 3. The variation range and calibrated values of the parameters describing soil hydraulic
705 characteristics and irrigation and drainage system.

Parameters	Description	Value range		Calibrated value
		Min	Max	
K_e	Soil evaporation coefficient, (-)	0.1	0.35	0.25
η_{lc}	Water utilization coefficient of lateral canal, (-)	0.81	0.91	0.88
η_{fc}	Water utilization coefficient of field canal, (-)	0.81	0.86	0.89
S_y	Specific yield, (-)	0.02	0.15	0.15
γ_d	Drainage coefficient, (-)	0.02	0.06	0.03
K	Permeability coefficient of unconfined aquifers, (mm/day)	731	12701	1150
A	Soil water permeability coefficient, (-)	0.7	3.4	3.4
m	Soil water permeability exponent, (-)	0.3	0.5	0.5

706

https://doi.org/10.5194/hess-2019-359
Preprint. Discussion started: 12 August 2019

Hydrology and Earth System Sciences
Discussions

Figure Captions

Fig.1. Schematic diagram of the conceptual RIWP model and the coupling between its sub-modules.

Fig.2. Schematic diagram of groundwater lateral runoff exchange between HRUs.

Fig.3. Schematic diagram of coupling soil water and salt dynamics, and groundwater level and salinity. And the IWP evaluation in each HRU.

Fig.4. Procedure chart of regional irrigation water productivity simulation.

Fig.5. Location of the Jiefangzha Irrigation District.

Fig.6. Relationship between the simulated and measured values during the crop growing season in calibration and validation period.

Fig.7. The comparison of the simulated and measured groundwater table depth for 4 typical sites during the crop growing season in the years of 2006-2013. (Note: a- uncultivated area during the years of 2006-2013; b- uncultivated area from 2006-2008, and sunflower field and maize field from 2009-2013; c, d- sunflower, wheat and maize field in the years of 2006-2013)

Fig.8. Parameter sensitivity analysis results of model for the three output variables: (a) irrigation water productivity, (b) groundwater table depth and (c) groundwater salinity.

Fig.9. Spatial distribution of irrigation water productivity for the three main crops during the period of 2006-2013. Each line shows the RIWP for each year by ascending order. The left, middle and right column shows the RIWP of wheat, sunflower and maize, respectively.

Fig.10. (a) Simulated regional irrigation water productivity under various groundwater table depth (h_g) conditions with different irrigation water amount (I_n) applied, and (b) its statistical analysis results. In Fig.10a, W, S and M represents wheat, sunflower and maize, respectively

https://doi.org/10.5194/hess-2019-359
Preprint. Discussion started: 12 August 2019

Hydrology and Earth System Sciences
Discussions
Open Access
EGU

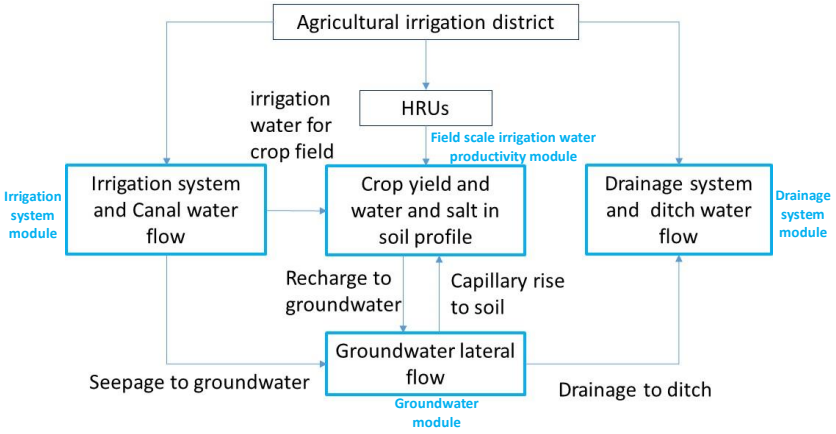

735

736 **Fig.1.** Schematic diagram of the conceptual RIWP model and the coupling between its sub-

737 modules.

738

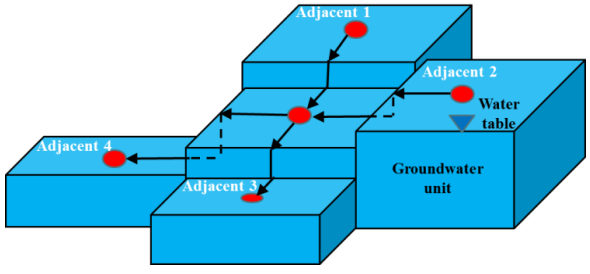

739

740 **Fig.2.** Schematic diagram of groundwater lateral exchange between adjacent HRUs.

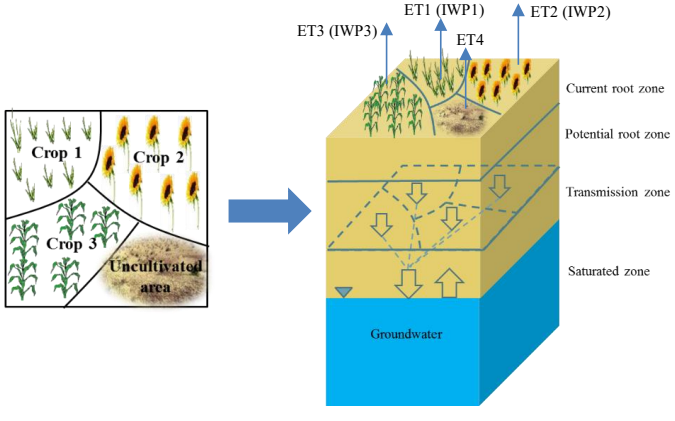

741

742 **Fig.3.** Schematic diagram of coupling soil water and salt dynamics, and groundwater level and

743 salinity. And the IWP evaluation in each HRU.

https://doi.org/10.5194/hess-2019-359
Preprint. Discussion started: 12 August 2019

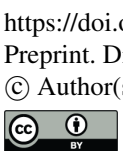

Hydrology and Earth System Sciences
Discussions

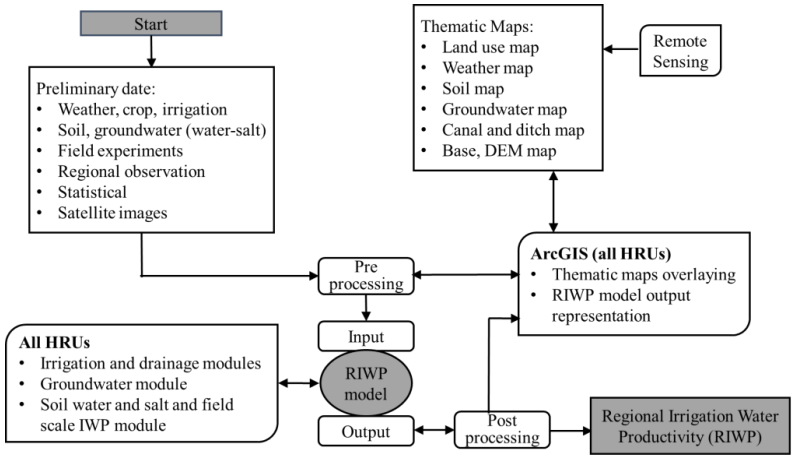

744

745 **Fig.4.** Procedure chart of regional irrigation water productivity simulation.

746

747

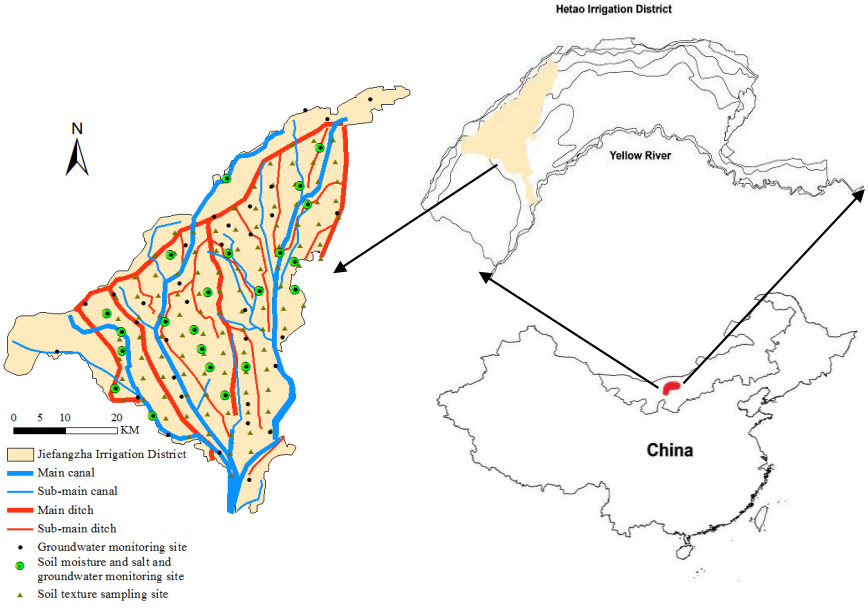

748

749 **Fig.5.** Location of the Jiefangzha Irrigation District.

750

751

752

753

https://doi.org/10.5194/hess-2019-359
Preprint. Discussion started: 12 August 2019

Hydrology and Earth System Sciences
Discussions

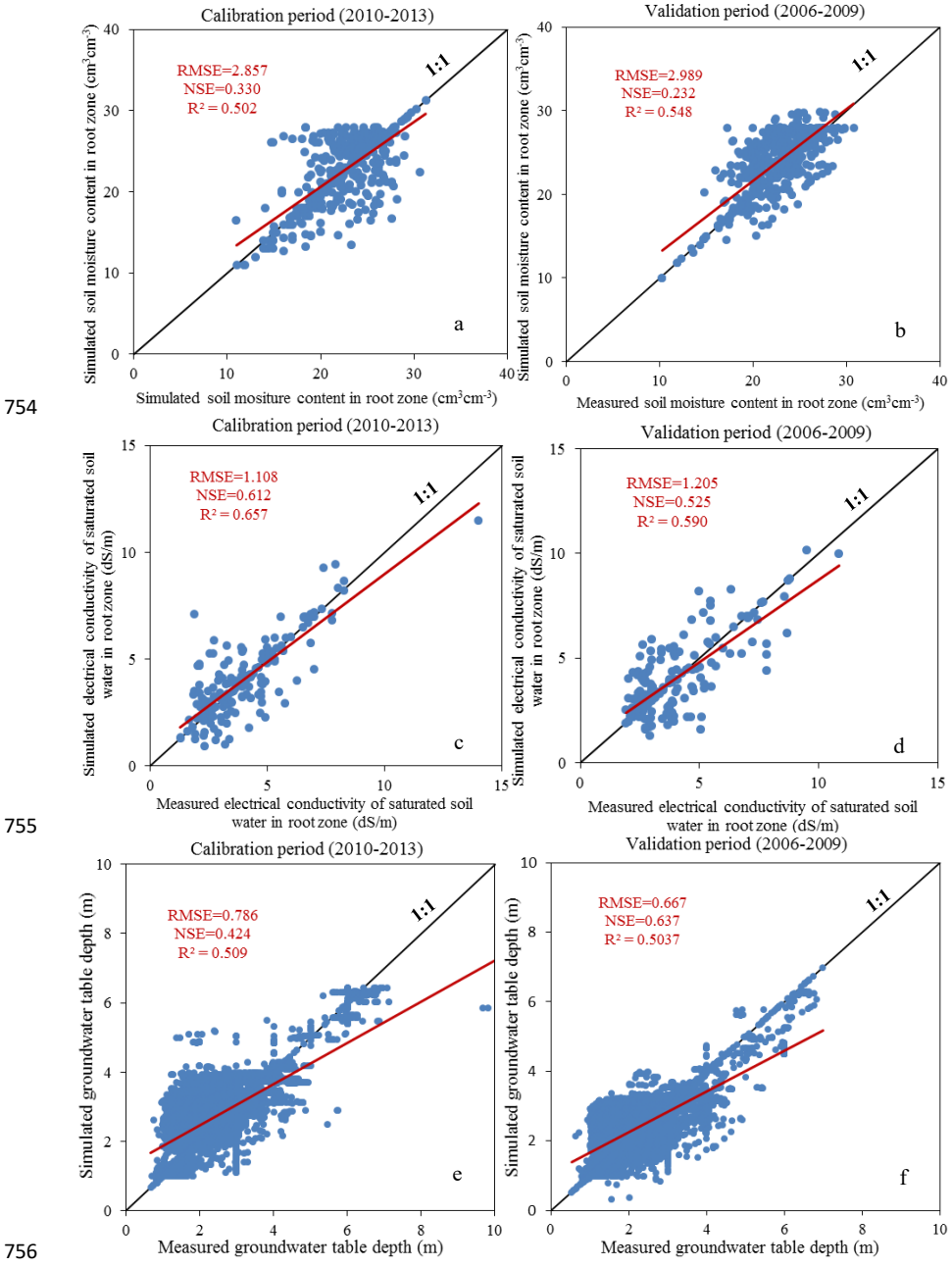

https://doi.org/10.5194/hess-2019-359
Preprint. Discussion started: 12 August 2019

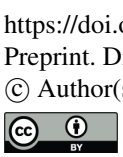

Hydrology and Earth System Sciences
Discussions

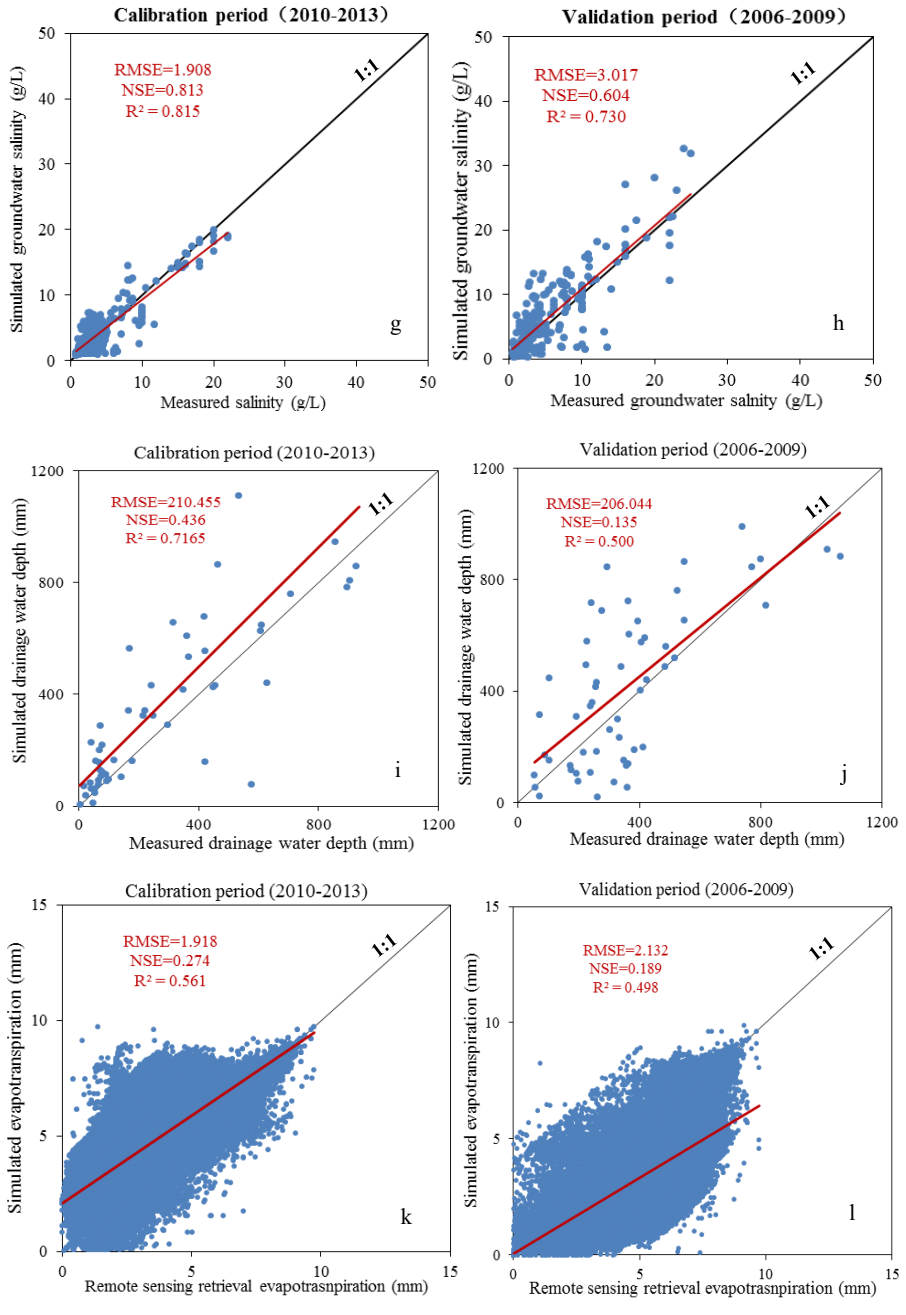

757
758
759

760 **Fig.6.** Relationship between the simulated and measured values during the crop growing season in
761 calibration and validation period.

https://doi.org/10.5194/hess-2019-359
Preprint. Discussion started: 12 August 2019

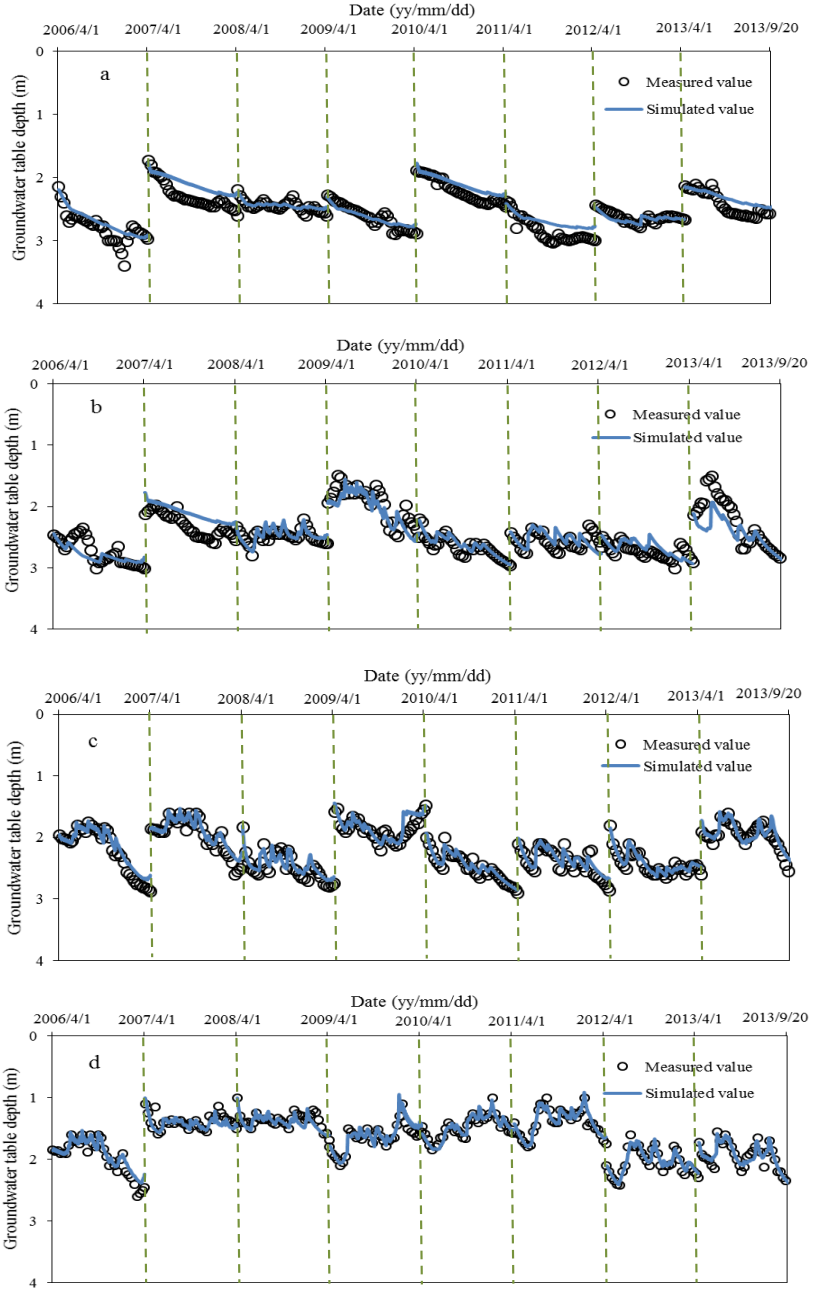

Fig.7. The comparison of the simulated and measured groundwater table depth for 4 typical sites during the crop growing season in the years of 2006-2013. (Note: a- uncultivated area during the years of 2006-2013; b- uncultivated area from 2006-2008, and sunflower field and maize field from 2009-2013; c, d- sunflower, wheat and maize field in the years of 2006-2013)

https://doi.org/10.5194/hess-2019-359
Preprint. Discussion started: 12 August 2019

Hydrology and Earth System Sciences
Discussions

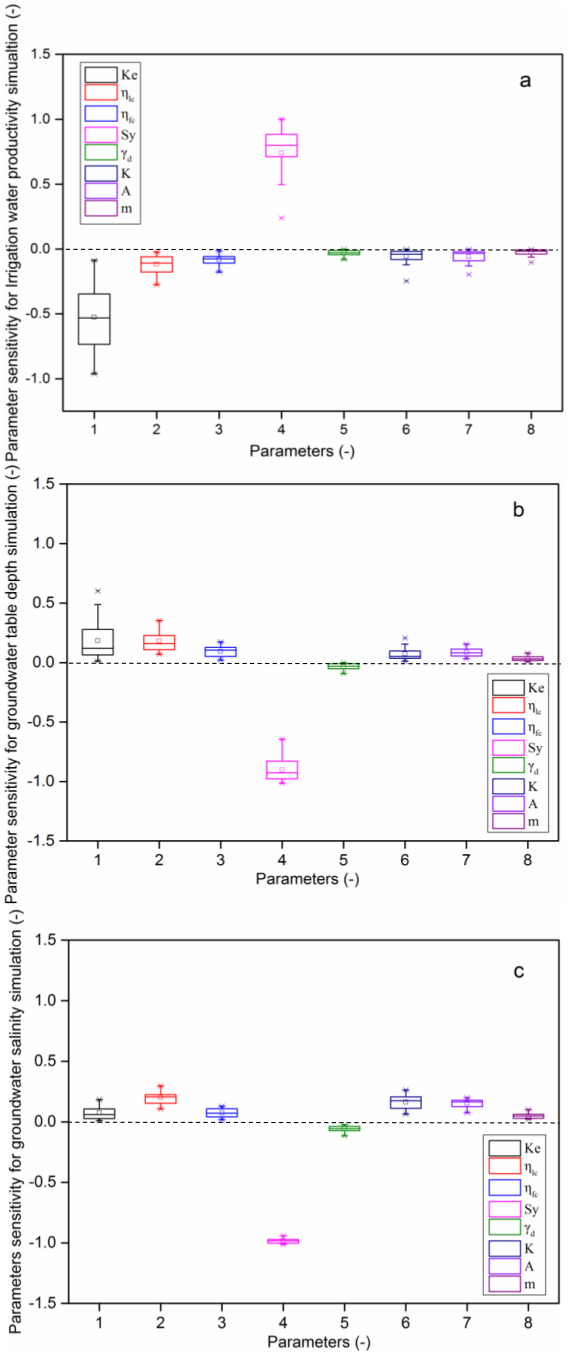

770

771

772

773 **Fig.8.** Parameter sensitivity analysis results of model for the three output variables: (a) irrigation

774 water productivity, (b) groundwater table depth and (c) groundwater salinity.

https://doi.org/10.5194/hess-2019-359
Preprint. Discussion started: 12 August 2019

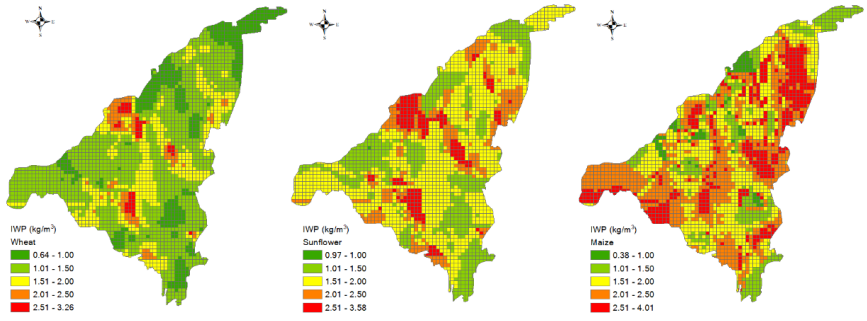

775

776 (a)

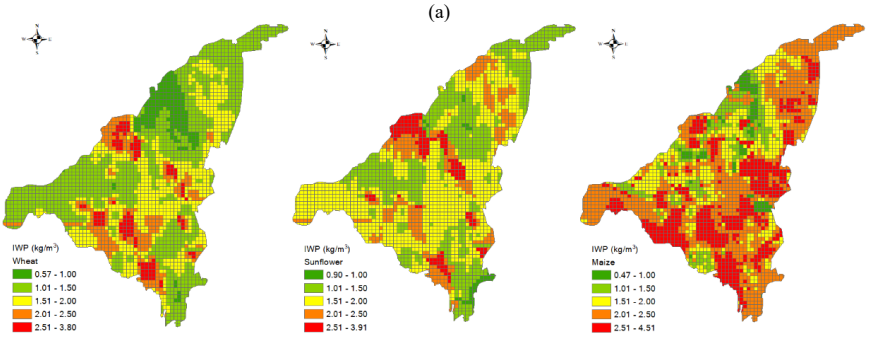

777

778 (b)

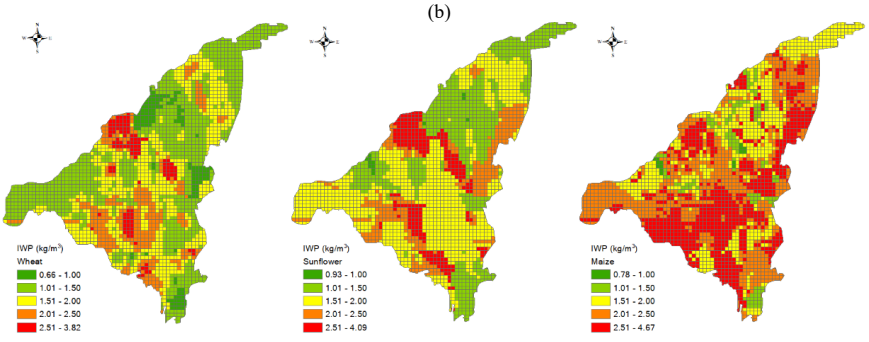

779

780 (c)

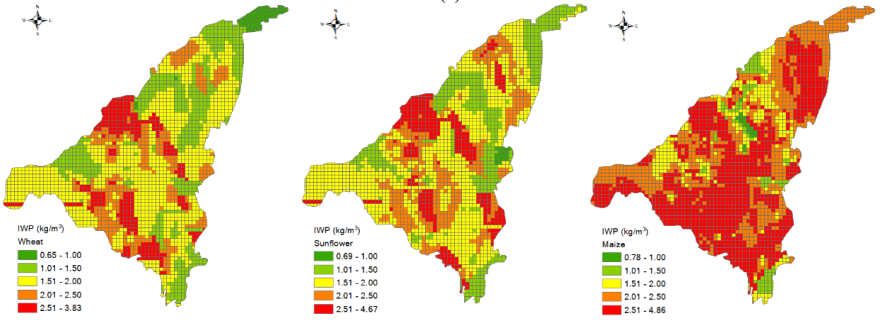

781

782 (d)

https://doi.org/10.5194/hess-2019-359
Preprint. Discussion started: 12 August 2019

Hydrology and Earth System Sciences
Discussions

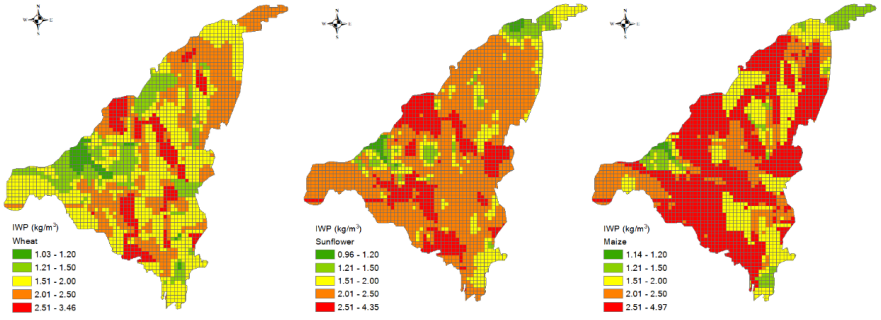

(e)

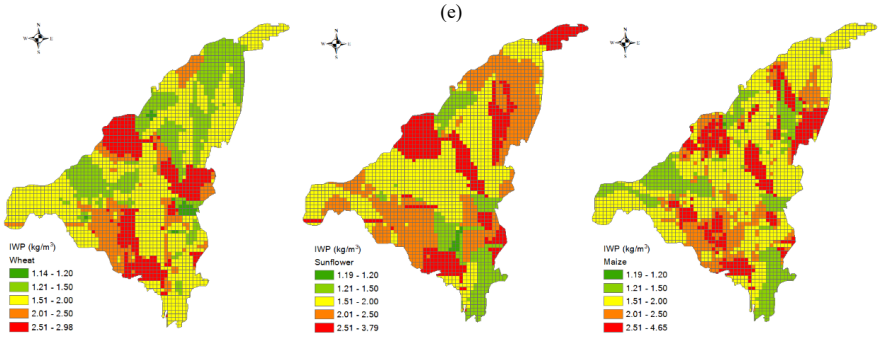

(f)

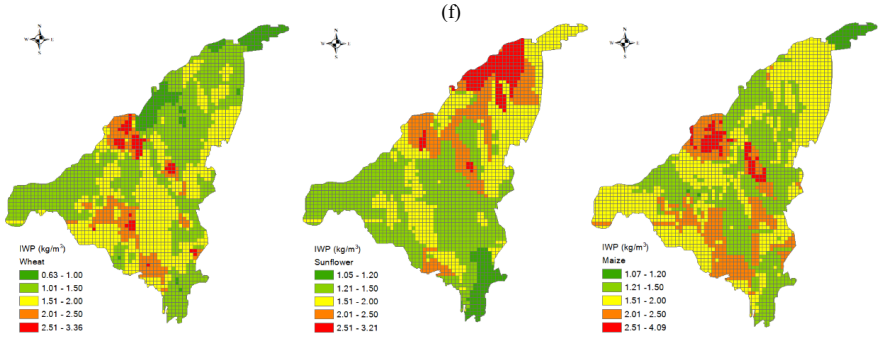

(g)

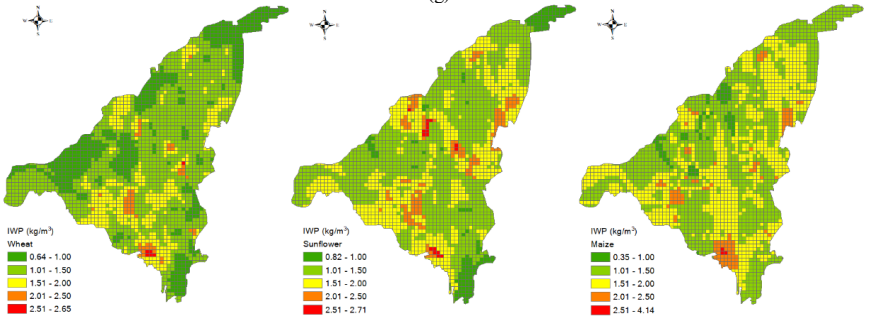

(h)

Fig.9. Spatial distribution of irrigation water productivity for the three main crops during the

https://doi.org/10.5194/hess-2019-359
Preprint. Discussion started: 12 August 2019

Hydrology and Earth System Sciences
Discussions

period of 2006-2013. Each line shows the RIWP for each year by ascending order. The left, middle and right column shows the RIWP of wheat, sunflower and maize, respectively.

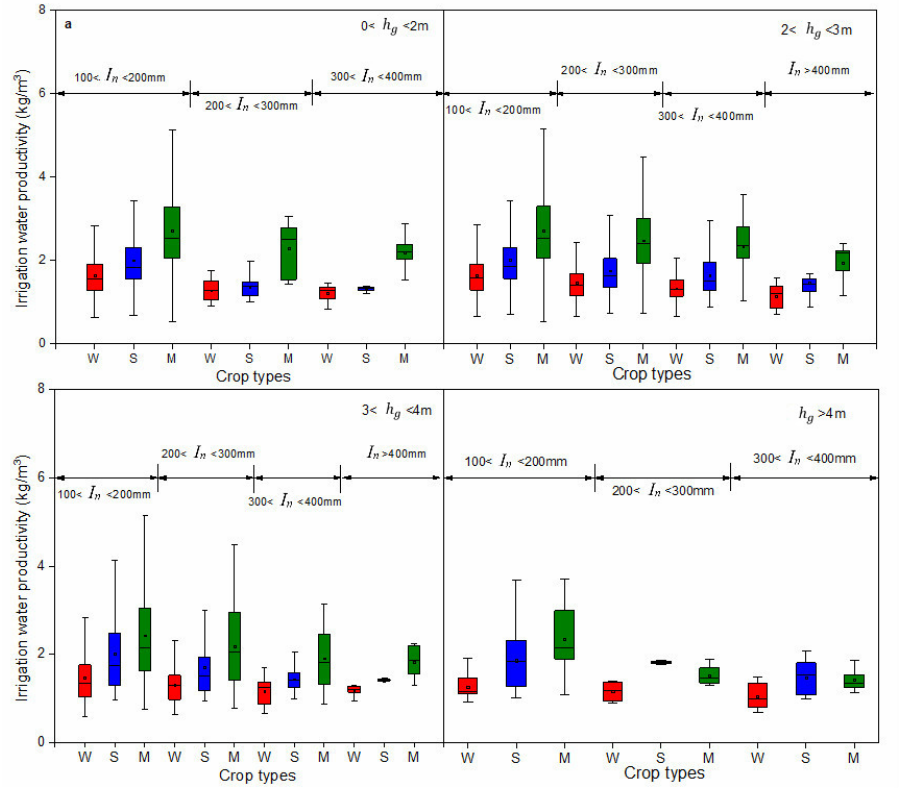

Fig.10. (a) Simulated regional irrigation water productivity under various groundwater table depth (h_g) conditions with different irrigation water amount (I_n) applied, and (b) its statistical analysis results. In Fig.10a, W, S and M represents wheat, sunflower and maize, respectively.